Int. J. Electrochem. Sci., 17 **(2022)** Article Number: 220331, doi: 10.20964/2022.03.35

International Journal of
ELECTROCHEMICAL
SCIENCE
www.electrochemsci.org

Electrochemical Sensor Based on Three-Dimensional rGO/ZnO composite for dopamine detection

Cuijie Nong, Bo Yang, Xiaokun Li, Suxiang Feng, Hongxin Cui*

School of Pharmacy, Henan University of Traditional Chinese Medicine, Zhengzhou 450046, China
*E-mail: li96052122@126.com

Received: 4 December 2021 / *Accepted:* 11 January 2022 / *Published:* 2 February 2022

In this study, a novel dopamine (DA) electrochemical sensor was designed based on three-dimensional reduced graphene oxide (3D rGO) and zinc oxide (ZnO). The morphologies and structures of 3D rGO and 3D rGO–ZnO were characterized via scanning electron microscopy, infrared spectrophotometry, and X-ray diffraction. Electrochemical impedance spectroscopy, cyclic voltammetry, and differential pulse voltammetry were used to investigate the electrochemical behavior of DA on the 3D rGO–ZnO/glassy carbon electrode (GCE). The results showed that the 3D rGO–ZnO/GCE improved electron transferability. In a phosphate-buffered solution with pH 7.0, the 3D rGO–ZnO/GCE exhibited an excellent catalytic activity for DA oxidation. In the ranges of 0.01–70 μM and 70–500 μM, the peak current exhibited an excellent linear relationship with DA concentration and the detection limit was 0.06 nM. The proposed sensor has high sensitivity, low-detection limit, and a wide linear range and can be used as an alternative analytical tool to detect DA in real samples.

Keywords: three-dimensional graphene, zinc oxide, electrochemical sensor; dopamine

1. INTRODUCTION

Dopamine (DA), a catechol substance, is an important neurotransmitter playing an indispensable role in the cardiovascular system, central nervous system, kidneys, and endocrine system [1,2]. Low or high levels of DA are associated with schizophrenia, Parkinson's disease, attention deficit hyperactivity disorder, and autism [3–5]. Currently, the detection of DA levels has become an important research topic. Recently, detection technologies such as high-performance liquid chromatography (HPLC) [6], ultraviolet–visible spectrophotometry [7], fluorometry [8], capillary electrophoresis [9], and electrochemical sensors [10] have been used in DA detection. Among these methods, Electrochemical methods are widely used because of their simple technology, low cost, high reproducibility, and high sensitivity.

As a two-dimensional (2D) material, graphene comprises sp^2 hybridized carbon atoms [11]. It has been broadly applied in the fields of electrochemical as well as photoelectric sensing [12,13], transparent conductors [14], and energy storage [15] due to its excellent properties, such as large specific surface area, good hydrophilicity, and excellent chemical stability [16]. However, the strong π–π interaction between graphene sheets makes graphene easy to accumulate and difficult to disperse in water [17]. Three-dimensional reduced graphene oxide (3D rGO), a member of the graphene family, is a 3D porous network aggregate assembled by 2D graphene, and its 3D network structure can effectively solve the agglomeration phenomenon caused by stacking graphene sheets [18,19]. In this experiment, 3D rGO/zinc oxide (3D rGO/ZnO) composites were prepared for detecting DA. This material shows excellent electrochemical performance in the detection of DA hydrochloride. Due to excellent optical and electrochemical properties, zinc oxide (ZnO), a p-type semiconductor material, has a bandgap of 3.37 eV [20] and is widely used in optoelectronic devices [21], catalysis [22], and electrochemical as well as photoelectrochemical sensing [23,24]. Presently, studies about ZnO-modified 3D rGO have been reported; however, the electrochemical detection of DA hydrochloride has not been reported in the literature. Therefore, in this work, 3D rGO–ZnO was selected for DA hydrochloride detection.

3D rGO–ZnO nanocomposites were synthesized and characterized via scanning electron microscopy (SEM), X-ray diffraction (XRD), and infrared spectrophotometry (IR). The synthesized material was modified on a glassy carbon electrode (GCE) to prepare an electrochemical sensor for the determination of DA in actual samples.

2. EXPERIMENT

2.1. Reagents

Hexamethylenetetramine (HMTA) and polyethyleneimine were purchased from Shanghai Aladdin Biochemical Technology Co., Ltd (Shanghai, China). DA was purchased from Shanghai Macleans Biochemical Technology Co., Ltd (Shanghai). Methanol, phosphoric acid, and N, N-dimethylformamide were purchased from Taicang Shanghai Testing Agent Co., Ltd (Taicang). Zinc acetate dihydrate and zinc nitrate hexahydrate were purchased from Tianjin Damao Chemical Reagent Co., Ltd (Tianjin). DA hydrochloride injection was purchased from Shanghai Harvest Pharmaceutical Co., Ltd (Shanghai, China). Human serum samples were provided from three adults in hospital (Beijing, China).

2.2. Instrument

A freeze dryer (FD-1D-50, Beijing Boyikang Experimental Instrument Co., Ltd.) and a tube furnace (GSL-1100X, Hefei Kejing Material Technology Co., Ltd.) were used to synthesize 3D rGO and 3D rGO–ZnO. Fourier transform IR spectrometry (FTIR PerkinElmer-65, USA), XRD (Bruker D8 Advance, Germany), and SEM (EV018, ZEISS, Germany) were used to study the structure and morphology of 3D rGO and 3D rGO–ZnO. An electrochemical workstation (CHI760, Shanghai Chenhua

Instrument Co., Ltd.) was used for all electrochemical measurement processes.

2.3. Synthesis of 3D rGO–ZnO

2.3.1 Synthesis of 3D rGO

Graphene oxide flakes (0.1 g) were dispersed in a beaker containing deionized water (100 mL) and sonicated for 5 h. This solution (20 mL) was removed to freeze dry for 36 h and then calcined at 500°C for 1 h under nitrogen protection to obtain 3D rGO.

2.3.2 Synthesis of 3D rGO-ZnO

Zinc acetate dihydrate (10 mL, 0.01 M) was added into methanol (10 mL) and stirred for 2 h. This solution was added to an alumina crucible containing a 3D rGO substrate and then placed in a tube furnace at 200°C for 20 minutes to obtain a seeded layer of ZnO nanocrystals.

Zinc nitrate hexahydrate (20 mL, 0.05 M) was mixed with HMTA (20 mL, 0.05 M) and stirred for 5 h; afterward, polyethyleneimine solution was added to the above solution. The pH of the aqueous solution was adjusted to 7–8. The previously prepared 3D rGO containing ZnO nanoseed crystals was added to the mixture, stirred for 30 min, transferred to a stainless-steel autoclave, and reacted at 90°C for 12 h. After the reaction, the product was washed with anhydrous alcohol and deionized water and dried at 60°C for 4 h. The synthesis process of 3D rGO and 3D rGO–ZnO is shown in Scheme 1.

2.4. Preparation of modified electrodes

First, the GCE was polished using 0.3 and 0.05 mM alumina powder and dried naturally. Then, 6 μL of 3D rGO–ZnO (2 mg/L in DMF) was dripped onto the electrode surface to obtain 3D rGO–ZnO/GCE. The 3D rGO/GCE and bare GCE were obtained by the same method. The construction process of the electrochemical sensor is shown in Scheme 1.

2.5. Electrochemical measurement

In this experiment, electrochemical impedance spectroscopy (EIS), cyclic voltammetry (CV), and differential pulse voltammetry (DPV) were used for determination and analysis of DA hydrochloride and a three-electrode system was used for the determination and analysis of DA hydrochloride in 0.2 M phosphate buffered solution (PBS).

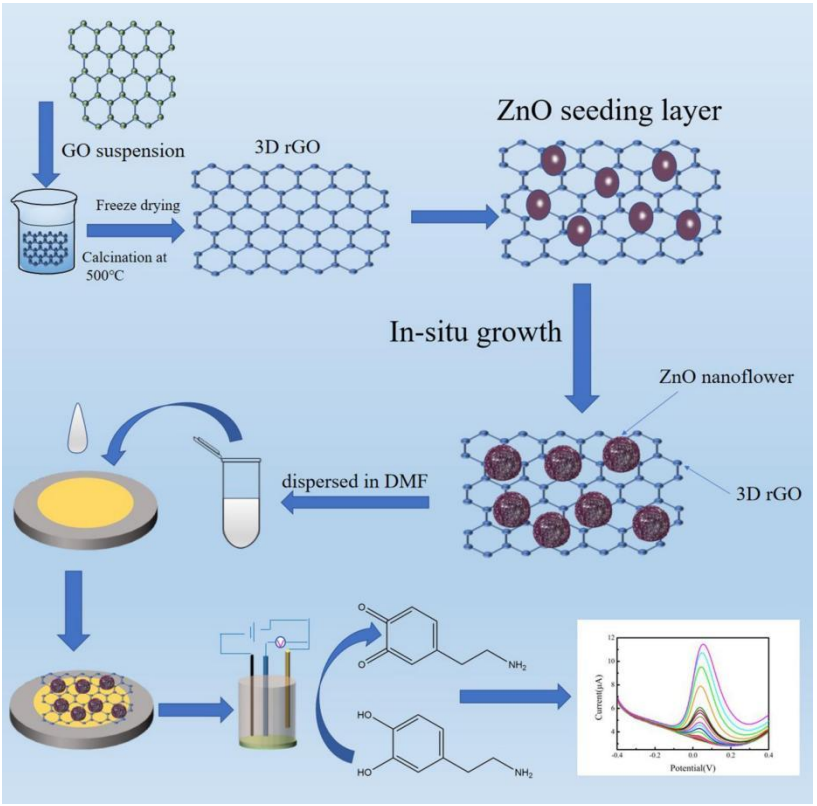

Scheme 1. Synthesis of composite materials and construction of the DA electrochemical sensor

3. RESULTS AND DISCUSSION

3.1. Characterization

SEM, XRD, and IR were used to characterize the morphologies and elements of 3D rGO and 3D rGO-ZnO. The 3D rGO presents a 3D reticular sheet structure in Fig. 1A. SEM images of 3D rGO-ZnO nanocomposites are shown in Fig. 1B, and the flower-like structure of ZnO is embedded in the 3D rGO structure.

Fig. 1C shows the XRD spectra of 3D rGO and 3D rGO–ZnO. In the 3D rGO spectrum, the characteristic diffraction peak of 3D rGO oxygen-containing functional groups appeared at about 8° and the characteristic diffraction peaks of graphitic carbon appeared at 30° and 43°, indicating successful synthesis of 3D rGO. In the 3D rGO–ZnO spectrum, the characteristic diffraction peaks of 3D rGO appeared at 30° and 43° and the characteristic diffraction peak of ZnO appeared at 25°.

Fig. 1D shows the IR spectra of 3D rGO and 3D rGO–ZnO. In the IR spectrum of 3D rGO, the absorption peaks at 3500, 1640, and 1350 cm^{-1} are attributed to the vibrational absorption peaks of the O–H, C=C, and C–OH bonds [24] respectively, indicating the successful synthesis of 3D rGO. For 3D rGO–ZnO, the characteristic absorption peaks of 3D rGO appear at 3500, 1600, 1400, and 500 cm^{-1}. The absorption peak at 800 cm^{-1} is assigned to ZnO [25]. The IR results showed the successful synthesis of 3D rGO–ZnO.

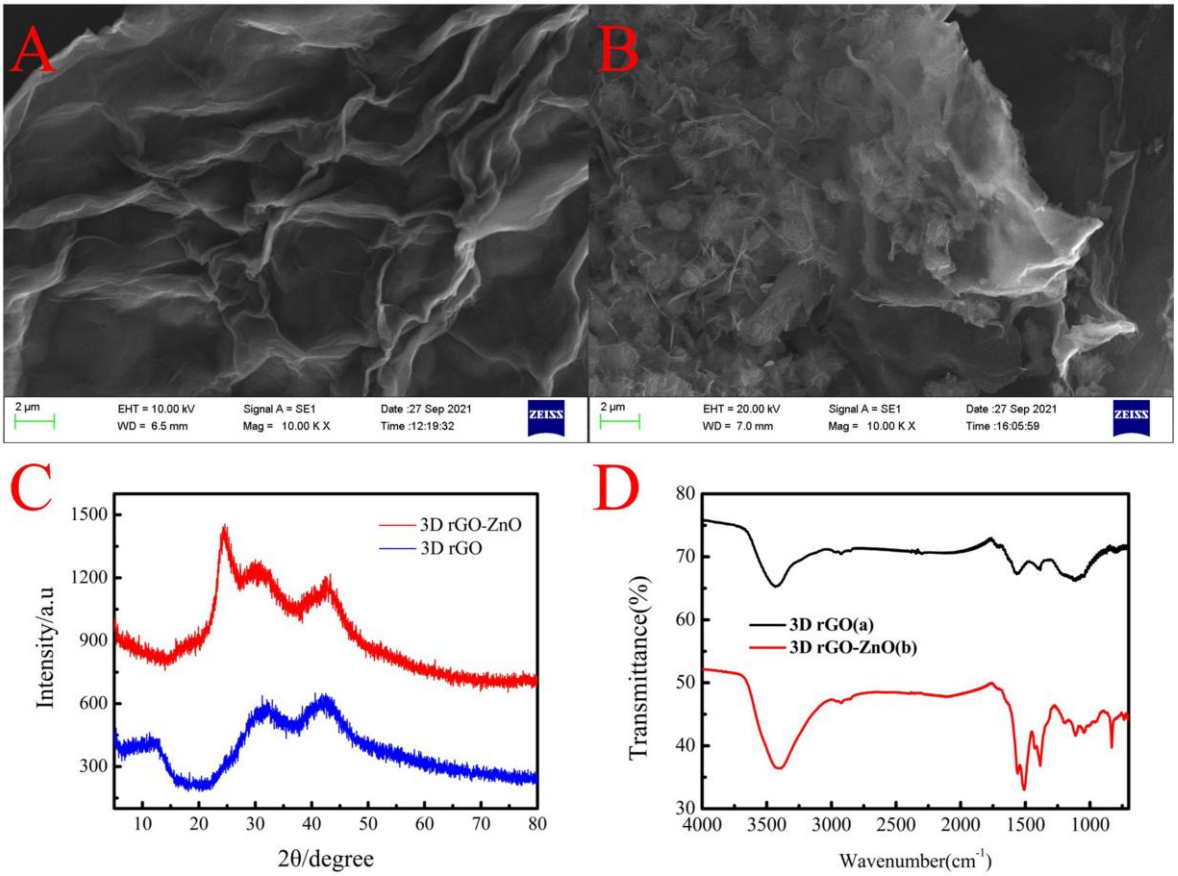

Figure 1. SEM images of 3D rGO (A) and 3D rGO–ZnO (B), XRD spectra of 3D rGO and 3D rGO–ZnO (C), and IR spectra of 3D rGO and 3D rGO–ZnO (D).

3.2. Electrochemical impedance analysis

In a 5.0-mM $[Fe(CN)_6]^{3-/4-}$ solution containing 0.1-M KCl, the charge transfer behaviors of the bare GCE, 3D rGO/GCE, and 3D rGO–ZnO/GCE were studied via EIS. The semicircle of the high-frequency region is due to the charge transfer resistance (Rct) in EIS, which reflects the electron transferability of the modified electrode, and the radius of the semicircle is equivalent to this resistance [26]. The Nyquist plots of the bare GCE, 3D rGO/GCE, and 3D rGO–ZnO/GCE are shown in Fig. 2A. The Rct of the 3D rGO/GCE was much larger than that of the bare GCE, indicating the low conductivity of 3D rGO compared with that of the bare GCE, which may be caused by the poor conductivity of 3D rGO. After the addition of ZnO, the Rct of 3D rGO–ZnO/GCE decreased significantly, indicating the strong electron transfer of 3D rGO–ZnO.

3.3. Timed Coulomb Analysis

The chronocoulometric method was used to study the chronocoulometric behavior of the bare GCE, 3D rGO/GCE, and 3D rGO–ZnO/GCE in a 1-mM $[Fe(CN)_6]^{3-/4-}$ solution containing 0.1-M KCl. Fig. 2C and 2D shows the Qt and $Qt^{1/2}$ diagrams of bare GCE, 3D rGO/GCE, and 3D rGO–ZnO/GCE,

respectively. The curve equations are $Q = 235.87t^{1/2}-17.44$ ($r = 0.99837$), $Q = 265.26t^{1/2}-14.795$ ($r = 0.99864$), and $Q = 277.79t^{1/2}-4.76$ ($r = 0.99823$), respectively. According to the Anson equation [27] and linear slope, the effective surface areas of the bare GCE, 3D rGO/GCE, and 3D rGO–ZnO/GCE are calculated to be 0.79, 0.88, and 0.93 cm^2, respectively. The results show a much larger effective surface area of the 3D rGO–ZnO/GCE than the 3D rGO/GCE. 3D rGO–ZnO/GCE improves the charge transfer in the reaction system, thereby enhancing the peak current.

3.4. Electrochemical behavior on different modified electrodes

The electrochemical behavior of 70-μM DA on the bare GCE, 3D rGO/GCE, and 3D rGO–ZnO/GCE was investigated by CV in PBS solution (10 mL, pH 7, 0.2 M). Fig. 2B shows the results of CV behavior on different modified electrodes. Neither the bare/GCE nor the 3D rGO/GCE showed a change in the current signal, whereas the 3D rGO–ZnO/GCE showed an obvious change in the current response, indicating that the prepared electrochemical sensor can be used to detect DA.

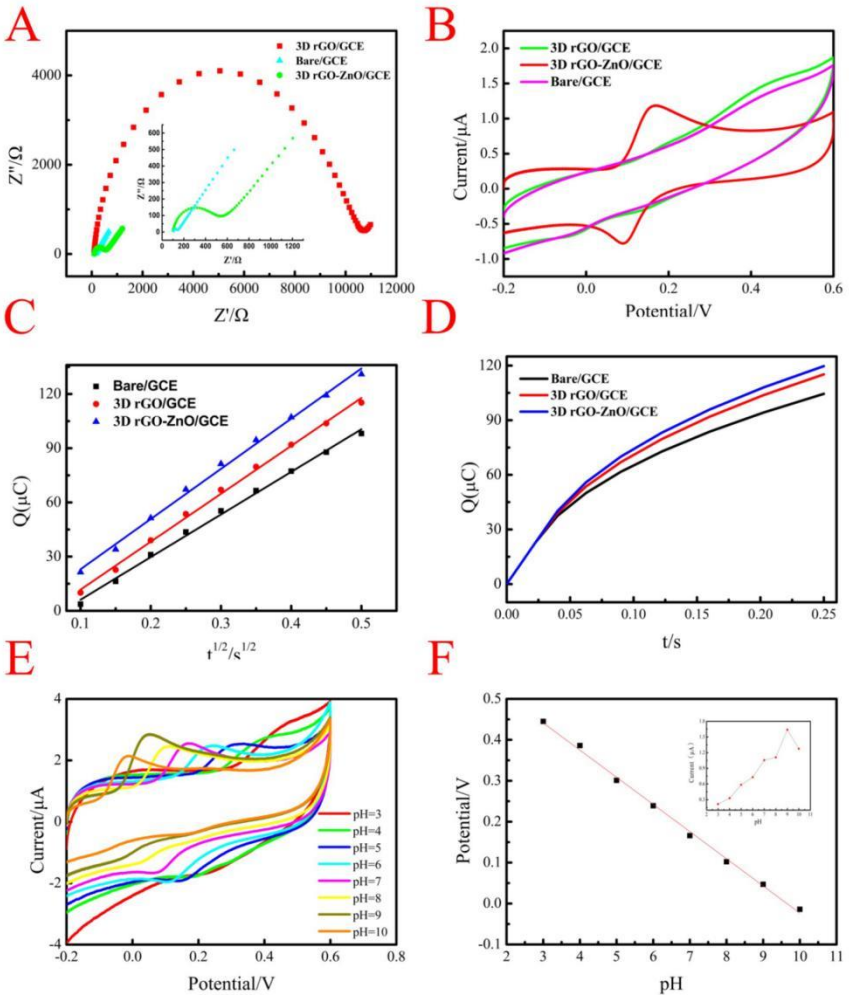

Figure 2. (A) EIS and (B) CV of different modified electrodes, (C) chronocoulometric curves, and (D) the corresponding $Qt^{1/2}$ plots of the various electrodes. (E) CV response of the 3D rGO–ZnO/GCE electrode at different pH (3–10) and (F) the relationship between pH and current as well as pH and potential.

3.5. Condition optimization

Electrochemical detection conditions were determined by optimizing the material concentration and buffer pH. In this work, the current response of DA on the 3D rGO–ZnO/GCE was analyzed via CV in the PBS solution with different pH ranges of 3.0–10.0 (Fig. 2E). The maximum CV response of the sensor was pH 9, which was used as the pH value for all subsequent experiments. Furthermore, the concentrations of 3D rGO–ZnO (0.5, 1.0, 1.5, 2.0, 2.5, and 3.0 mg) were studied (Fig. 3A). The CV response of DA first increased and then decreased, and the current response reached a maximum at 2.0 mg/mL with an increase in the 3D rGO–ZnO concentration. The decrease in CV response may be due to the obstruction of electron transfer caused by the increase in film thickness. Therefore, 2.0 mg/mL 3D rGO–ZnO was selected to prepare the electrochemical sensor.

3.6. Study of the scan rate

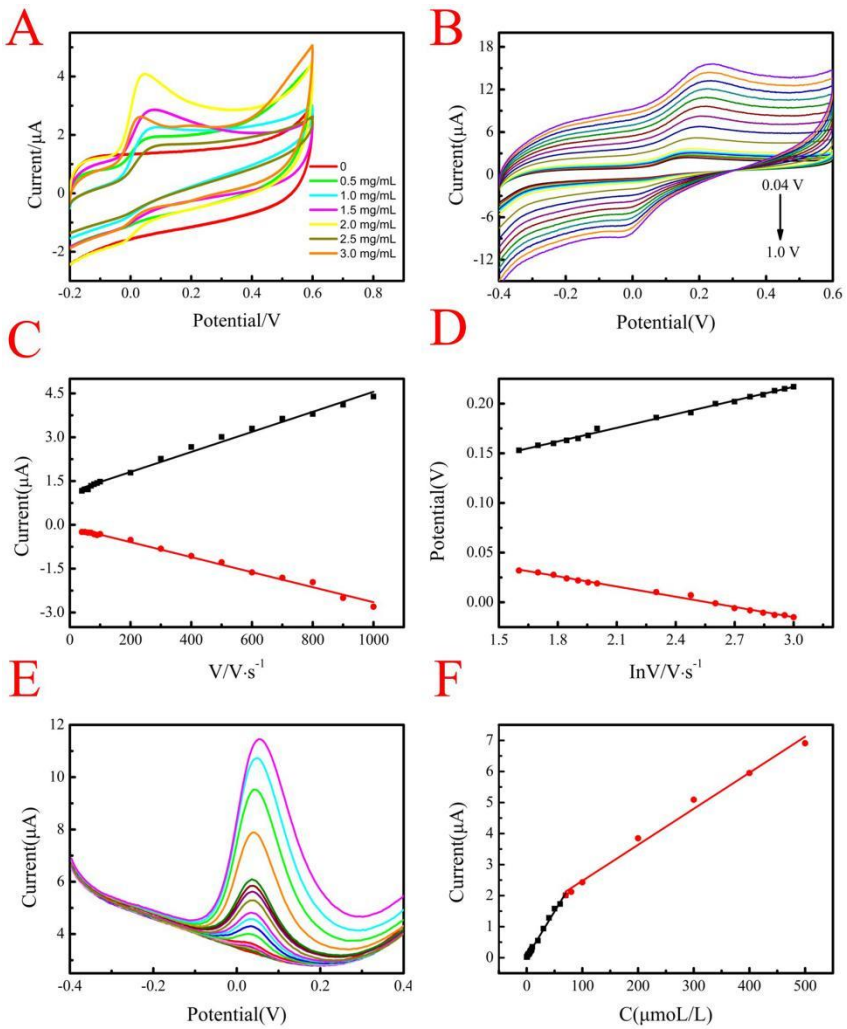

Figure 3. (A) CV response of DA at different concentrations of the 3D rGO–ZnO modified electrode. (B) CVs of different scan rates in the range of 0.3–1.0 V/s. (C) Relation between peak currents versus scan rate. (D) Relationship between peak potential and the square root of scanning rate. (E) DPV curves and (F) linear relationship of DA detection.

Under optimal conditions, the electrochemical behavior of DA on the 3D rGO–ZnO/GCE was investigated via CV at different scan rates. As shown in Fig. 3B, the oxidation and reduction peak currents of DA increased with an increase in the scanning rate and showed a linear correlation in the range of 0.04–1.0 V. Their linear equations were Ipa = $3.43C_{DA}$ + 1.125 (r = 0.9959) and Ipc = $-2.57C_{DA}$ − 0.0775 (r = 0.9912), respectively. The potential (Ep) of DA has a linear relationship with the logarithm of scan velocity (lnv). The linear equations were Epa = 0.079 + 0.045 lnv (V/s) and Epc = 0.087–0.034 lnv (V/s), and the correlation coefficients were 0.9959 and 0.9936, respectively. The results showed that DA has a good electron transfer effect on the 3D rGO–ZnO/GCE, indicating that the redox process is a process of adsorption control [29,30].

3.7. Electrochemical behavior of DA on the prepared sensor

The electrochemical behaviors of the prepared sensor were studied via DPV at different concentrations under optimal conditions. From Fig. 3E, the peak current of DA increases with an increase in the DA concentration. In the concentration ranges of 5 nM–70 μM and 70 μM–500 mM, a consistent linear relationship is observed (Fig. 3F). The linear equations are I_{P1} (μA) = 0.18526 + $0.0294C_{DA}$ (r = 0.99816) and I_{P2} (μA) = 13.1593 + $0.0116C_{DA}$ (r = 0.99616), with a detection limit of 0.6 nM. At low DA levels, even a small change in concentration will cause a significant change in the response signal due to the diffusion effect on the electrode surface. The local concentration on the electrode surface decreases rapidly as the 3D rGO–ZnO/GCE converts DA into a product when the DA concentration is low. In this case, the sensor shows high sensitivity. At a higher DA level, the interaction time between the material and the substrate is longer. This may be because the reaction products pollute the electrode surface, resulting in a low slope [30,31]. Therefore, the sensor shows two linear correlation coefficients at high and low concentration. Furthermore, the constructed sensor was compared with the reported DA sensor and the results are shown in Table 1.

Table 1. Comparison of the proposed sensor with other reported sensors used for dopamine determination

Electrode	Method	Linear range(μM)	Detection limit (μM)	Refs.
CuO nanodots-ITO[a]	DPV	0.12–56.87	0.03	[33]
GQDs[b]@MWCNTs[c]/GCE	DPV	0.25–250	0.095	[34]
N-G[d]/NiTsPc[e]/GCE	DPV	0.1–200	0.1	[35]
CoTAPc[f]-GO/Cu-Bi_2WO_6[g]/ITO	i-t	0.05–250	0.0072	[36]
Au@ZIF-8[h]/GCE	DPV	0.1–50	0.01	[37]
3D rGO-ZnO/GCE	DPV	0.001–70,70–500	0.0006	This work

a) Indium tin oxide-coated glass slide; b) graphene quantum dots; c) multiwalled carbon nanotubes; d) nitrogen-doped graphene; e) and f) tetraminocobalt phthalocyanine; g) copper-doped bismuth; and h) zeolitic imidazolate framework-8

3.8. Reproducibility, stability, and interference study

Simultaneously, five independent 3D rGO–ZnO/GCEs were prepared and DPV was performed to study the repeatability of the sensor under optimal conditions. The results indicate that the peak current values were not significantly different and the RSD of the peak current was 0.34%, indicating good reproducibility of the prepared sensor.

DPV was conducted to study the stability of the electrochemical sensor in a PBS solution containing 70 μM DA. After the first day of testing, the 3D rGO–ZnO/GCEs were stored in the refrigerator and tested every 3 days (15 days as a cycle) with three parallel tests each time. The RSD of the peak current and the initial current was 3.97%. The experimental results showed that the 3D rGO–ZnO/GCE has good stability.

Under suitable experimental conditions, DPV was performed to study the interference effects of organic compounds, metal ions, inorganic salt ions, and some auxiliary components of drugs on DA in a PBS containing 70 μM DA. The results showed that the relative error between these interfering substances and DA hydrochloride was less than ±5%, and the impact of this error was negligible.

3.9. Real sample analysis

The content of DA in the injection was determined to assess the suitability of the 3D rGO–ZnO/GCE sensor for clinical sample detection. The accuracy of the experimental results has been expressed as a percentage labeled quantity. In addition, the DA content in the commercially available DA hydrochloride injection was determined by HPLC and compared with the results obtained using the proposed sensor (Table 2). The results of the two methods do not significantly differ.

Table 2. Results of the DA detection in the real sample under the optimal conditions (n = 5).

Sample	Labeled amount (mg/mL)	HPLC (mg/mL)	This work (mg/mL)	Percentage of labeled amount (%)	RSD (%)
DA hydrochloride injection	10	9.92	10.19	101.90	1.77

For human serum samples, the accuracy test results were expressed as recovery rates (Table 3). The constructed electrochemical sensor has a recovery rate of 96.5%–104.7% for DA detection in serum. Experimental results show that the constructed sensory organ has important practical significance for DA detection in actual clinical samples.

Table 3. Results of DA detection in serum samples

Sample	Added (μmol/L)	Found (μmol/L)	Recovery (%)	RSD (%, n =5)
Serum 1	2.0	1.9	96.5	4.0
Serum 2	4.0	4.1	104.7	5.0
Serum 3	8.0	7.9	101.2	2.0

4. CONCLUSION

Here, an electrochemical sensor composed of 3D rGO and ZnO nanocomposite materials was established for DA detection. First, the 3D rGO and 3D rGO–ZnO nanocomposite materials were synthesized and characterized by SEM, IR, and XRD. The sensor was prepared by dropping a 3D rGO–ZnO suspension (6 μL) on the GCE. The developed sensor demonstrated an excellent piecewise linear relationship and low-detection limit (0.6 nM) in the DA concentration ranges of 5 nM–70 μM and 70 μM–500 mM. In addition, this sensor exhibited outstanding repeatability and stability and can be used to determine the content of DA hydrochloride in DA hydrochloride injection, with a recovery rate of 96.5%–104.7%. As a result, the sensor can be used for the detection of DA and determination of its content in actual samples.

ACKNOWLEDGEMENTS
This study was supported by Zhong Jing Young Scholar Research Foundation of Henan University of Chinese Medicine(00104311-2021-1-12) and the 2020 postgraduate research and innovation project of Henan University of Traditional Chinese Medicine: the sensitive detection of cortisol based on the electrochemical sensor of MoS_2-AuNPs.

References

1. X.D. Xiao, L. Shi, L.H. Guo, J.W. Wang, X. Zhang, *Spectrochim. Acta - Part A Mol. Biomol. Spectrosc.*, 173 (2017) 6–12.
2. Y. Li, X. Liu, X. Zeng, X. Liu, B. Kong, W. Wei, S. Luo, *Electrochim. Acta*, 56 (2011) 2730–2734.
3. V. Voon, J. Gao, C. Brezing, M. Symmonds, V. Ekanayake, H. Fernandez, R.J. Dolan, M. Hallett, *Brain*, 134 (2011) 1438–1446.
4. I. Makkonen, R. Riikonen, H. Kokki, M.M. Airaksinen, J.T. Kuikka, *Dev. Med. Child Neurol.*, 50 (2008) 593–597.
5. D.Q.M. Madureira, L.A.V. Carvalho, E. Cheniaux, *Cognit. Comput.*, 2 (2010) 31–49.
6. H. Gu, E.L. Varner, S.R. Groskreutz, A.C. Michael, S.G. Weber, *Anal. Chem.*, 87 (2015) 6088–6094.
7. Q. Xu, J. Yoon, *Chem. Commun.*, 47 (2011) 12497–12499.
8. M. Chen, Y. Zheng, J. Gao, C. Li, C. Yu, Q. Wang, *Microchim. Acta*, 184 (2017) 2275–2280.

9. V. Šolínová, L. Žáková, J. Jiráček, V. Kašička, *Anal. Chim. Acta*, 1052 (2019) 170–178.
10. N. Roy, S. Yasmin, S. Jeon, *Microchem. J.*, 153 (2020) 104501.
11. X.C. Dong, H. Xu, X.W. Wang, Y.X. Huang, M.B. Chan-Park, H. Zhang, L.H. Wang, W. Huang, P. Chen, *ACS Nano*, 6 (2012) 3206–3213.
12. J. Peng, C. Hou, X. Hu, *Sensors Actuators, B Chem.*, 169 (2012) 81–87.
13. J. Peng, Q. Huang, W. Zhuge, Y. Liu, C. Zhang, W. Yang, G. Xiang, *Biosens. Bioelectron.*, 106 (2018) 212–218.
14. K.S. Kim, Y. Zhao, H. Jang, S.Y. Lee, J.M. Kim, K.S. Kim, J.H. Ahn, P. Kim, J.Y. Choi, B.H. Hong, *Nature*, 457 (2009) 706–710.
15. Y. Zhu, S. Murali, M.D. Stoller, K.J. Ganesh, W. Cai, P.J. Ferreira, A. Pirkle, R.M. Wallace, K.A. Cychosz, M. Thommes, D. Su, E.A. Stach, R.S. Ruoff, *Science (80-.).*, 332 (2011) 1537–1541.
16. J. Peng, Q. Huang, Y. Liu, P. Liu, C. Zhang, *Sensors Actuators, B Chem.*, 294 (2019) 157–165.
17. S. Stankovich, D.A. Dikin, R.D. Piner, K.A. Kohlhaas, A. Kleinhammes, Y. Jia, Y. Wu, S.B.T. Nguyen, R.S. Ruoff, *Carbon N. Y.*, 45 (2007) 1558–1565.
18. C. Song, X. Yin, M. Han, X. Li, Z. Hou, L. Zhang, L. Cheng, *Carbon N. Y.*, 116 (2017) 50–58.
19. F. Liu, Q. Xu, W. Huang, Z. Zhang, G. Xiang, C. Zhang, C. Liang, H. Lian, J. Peng, Electrochimica Acta, 295 (2019) 615-623.
20. Z.P. Shan, S.L. Gu, S.M. Zhu, W. Liu, K. Tang, H. Chen, J.G. Liu, Y.D. Zheng, *Appl. Surf. Sci.*, 254 (2008) 6962–6966.
21. R.J. Chung, Z.C. Lin, P.K. Yang, K.Y. Lai, S.F. Jen, P.W. Chiu, *Nanoscale Res. Lett.*, 8 (2013) 1–5.
22. M.M. Abdel-Mottaleb, A. Khalil, S.A. Karim, T.A. Osman, A.Khattab, *J. Mech. Behav. Biomed. Mater.*, 96 (2019) 118–124.
23. Q. Wang, H. Si, L. Zhang, L. Li, X. Wang, S. Wang, *Anal. Chim. Acta*, 1104 (2020) 69–77.
24. F. Khurshid, M. Jeyavelan, M.S.L. Hudson, S. Nagarajan, *R. Soc. Open Sci.*, 6 (2019).
25. W. Zhuge, X. Li, S. Feng, Microchem. J., 155 (2020) 104726.
26. R. Atchudan, T.N.J.I. Edison, S. Perumal, D. Karthikeyan, Y.R. Lee, J. Photochem. Photobiol. B Biol., 162 (2016) 500–510.
27. S. Chaiyo, E. Mehmeti, W. Siangproh, T.L. Hoang, H.P. Nguyen, O. Chailapakul, K. Kalcher, *Biosens. Bioelectron.*, 102 (2018) 113–120.
28. S. Hu, H. Zhu, S. Liu, J. Xiang, W. Sun, L. Zhang, *Microchim. Acta*, 178 (2012) 211–219.
29. E. Laviron, *J. Electroanal. Chem.*, 101 (1979) 19–28.
30. I. Ismail, T. Okajima, S. Kawauchi, T. Ohsaka, *Electrochim. Acta*, 211 (2016) 777–786.
31. X.X. Dong, M.Y. Li, N.N. Feng, Y.M. Sun, C. Yang, Z.L. Xu, *RSC Adv.*, 5 (2015) 86485–86489.
32. J.Y. Peng, C.T. Hou, X.X. Liu, H.B. Li, X.Y. Hu, *Talanta*, 86 (2011) 227–232.
33. S.Z. Bas, C. Cummins, A. Selkirk, D. Borah, M. Ozmen, M.A. Morris, *ACS Appl. Nano Mater.*, 2 (2019) 7311–7318.
34. S.K. Arumugasamy, S. Govindaraju, K. Yun, *Appl. Surf. Sci.*, 508 (2020) 145294.
35. H. Xu, J. Xiao, L. Yan, L. Zhu, B. Liu, *J. Electroanal. Chem.*, 779 (2016) 92–98.
36. J. Peng, W. Zhuge, Y. Liu, C. Zhang, W. Yang, Y. Huang, *J. Electrochem. Soc.*, 166 (2019) B1612–B1619.
37. S. Lu, M. Hummel, K. Chen, Y. Zhou, S. Kang, Z. Gu, *Electrochem. Commun.*, 114 (2020) 106715.